Materials Characterization 131 (2017) 425–430

Contents lists available at ScienceDirect

Materials Characterization

journal homepage: www.elsevier.com/locate/matchar

Simultaneously improving mechanical properties and damping capacity of Al-Mg-Si alloy through friction stir processing

H.J. Jiang[a], C.Y. Liu[a,b,*], B. Zhang[c], P. Xue[b], Z.Y. Ma[b,**], K. Luo[a], M.Z. Ma[c], R.P. Liu[c]

[a] Key Laboratory of New Processing Technology for Nonferrous Metal & Materials, Ministry of Education, Guilin University of Technology, Guilin 541004, China
[b] Shenyang National Laboratory for Materials Science, Institute of Metal Research, Chinese Academy of Sciences, 72 Wenhua Road, Shenyang 110016, China
[c] State Key Laboratory of Metastable Materials Science and Technology, Yanshan University, Qinhuangdao 066004, China

ARTICLE INFO

Keywords:
Al alloy
Friction stir processing
Mechanical properties
Damping

ABSTRACT

In this study, friction stir processing (FSP) was performed on an Al-Mg-Si alloy (AA 6082-T4) at a low tool rotation rate of 200 rpm, and good mechanical and damping properties were simultaneously obtained after FSP. The combination of excellent ductility, moderate strength and excellent room/high temperature damping capability at FSP sample was attributed to the ultrafine recrystallized grains with predominant high-angle grain boundaries and moderate dissolution of metastable phases, and the fragmentation of micron-sized second phase during FSP. This work provided an effective strategy to improve the damping capacity of commercial Al alloys without sacrificing their mechanical properties.

1. Introduction

Internal friction or damping capacity is defined as the capacity of a material to convert mechanical energy of vibrations into heat that is dissipated in the material. Damping capacity is receiving considerable attention given the increasing demand in vibration and noise control in modern industries [1,2].

Al alloys are widely used in aviation, aerospace, and civilian transport because of their excellent mechanical and physical properties [3]. However, Al alloys are regarded as low damping materials. Improving the damping capacity of Al alloys is especially important in the fabrication of equipment with low density, excellent mechanical properties, and sensitive to vibrations.

Three methods are mainly used to improve the damping capacity of Al materials in previous studies: 1) structure design, such as introducing high-density of macroscopic pores into Al matrixes to fabricate foamed Al [4]; 2) adding particles such as SiC [5], Al_2O_3 [6], TiB_2 [7], and NiTi [8] into Al matrixes to fabricate Al matrix composites (AMMCs); and 3) adding high-concentration of Zn (mass ratio usually > 70%) into Al matrix to fabricate Al-Zn alloys [9,10]. However, the above high damping Al materials usually show deteriorated mechanical properties such as low tensile strength or ductility compared with conventional Al alloys and are unable to replace commercial Al alloys in engineering fields. Therefore, more studies are needed to further improve the damping capacity of commercial Al alloys without sacrificing their mechanical properties.

The most important strategy to increase the room-temperature damping capacity of metals is controlling the presence and movement of dislocations [1]. The Granato–Lücke model [11] is often used to explain dislocation internal friction. In this case, the dissipation of mechanical energy is connected with the vibrations of dislocation segments. Solute atoms and vacancies (defined as weak pinning points) can effectively pin the dislocation segments at low vibration amplitude. Increasing the strain amplitude, dislocation segments break away from the weak pinning points but are still pinned by precipitates (defined as strong pinning points) [12,13].

The dislocation damping mechanism is weakened by increased temperature. The high-temperature damping capacity of Al alloys is mainly controlled by the interface between phases and grain boundary (GB) sliding behaviors, and excellent interface/GB sliding capacity usually corresponds to the high damping capacity [5,9].

So, according to the current internal friction theory, introduction of mobile dislocations or reducing pinning points such as solute atoms and precipitates can increase the room-temperature damping capacity of Al alloys. However, Al alloys with above structural characteristics always exhibit a poor mechanical property due to the low solid solution and precipitation strengthening effects. So, other strengthening effect is needed to improve the mechanical properties.

* Correspondence to: C.Y. Liu, Key Laboratory of New Processing Technology for Nonferrous Metal & Materials, Ministry of Education, Guilin University of Technology, Guilin 541004, China.
** Corresponding author.
E-mail addresses: lcy261@glut.edu.cn (C.Y. Liu), zyma@imr.ac.cn (Z.Y. Ma).

http://dx.doi.org/10.1016/j.matchar.2017.07.037
Received 21 April 2017; Received in revised form 2 July 2017; Accepted 19 July 2017
Available online 20 July 2017
1044-5803/

Grain refinement could improve the mechanical properties of Al alloys, such as strength and toughness. The Al alloys with fine grain structure usually exhibit superplasticity, which is attributed to the excellent GB sliding capacity [14–18]. As mentioned above, the high-temperature damping capacity of metals mainly depends on their GB sliding capacity [9]. So, the damping and mechanical properties of commercial Al alloys are expected to simultaneously improve by the grain refinement.

Friction stir processing (FSP) is an effective method of achieving grain refinement [15–19]. Furthermore, other microstructural characteristics, which deeply affect the mechanical properties and damping capacity of materials, such as the amount of solutes in solid solution, density of precipitates and dislocations can be also designed by FSP with heat input controlling [20].

In the present study, the effects of FSP with low rotation rate on the microstructure, mechanical properties and damping capacity of an Al-Mg-Si alloy were investigated. The aim is to fabricate commercial Al alloys with excellent damping capacity and mechanical properties by means of FSP.

2. Experimental Methods

The raw material was a commercial Al-Mg-Si alloy (AA 6082-T4) with a sheet thickness of 4 mm, obtained from Alnan Aluminum Co., Ltd. The chemical composition of the Al alloy was 0.77 Mg, 1.16 Si, 0.05 Cu, 0.27 Fe, 0.02 Cr, 0.68 Mn, 0.02 Ti, 0.04 Zn, and 0.01 Ni (wt%). FSP was conducted at a constant traverse speed of 50 mm min^{-1} with tool rotation rate of 200 rpm, defined as FSP sample. A tool with a concave shoulder 10 mm in diameter and a taper threaded pin 3.7 mm in length and 4 mm in diameter was used.

The microstructures of the samples were examined by optical microscopy (OM), electron backscattered diffraction (EBSD) and transmission electron microscopy (TEM, JEM-2010). The films for TEM were prepared by grinding to a thickness of 50 μm, followed by thinning using a twinjet electropolishing device.

Tensile tests were conducted on an Instron 5982-type testing machine at a strain rate of $4 \times 10^{-4}\ s^{-1}$. The specimens for tensile test were machined parallel to the FSP direction. The internal friction behavior (i.e., damping performance) of the samples was characterized using specimens with a dimension of 1.2 mm × 4 mm × 25 mm. Internal friction tests were conducted by a dynamic mechanical analyzer (Q800, TA) in single-cantilever mode. Measurements were made at strain amplitudes (ε) of 5×10^{-5} to 5×10^{-1}, temperatures (T) of 310 to 630 K with a heating rate of 5 K/min, and frequency (f) of 0.5 and 1 Hz.

3. Results and Discussion

Fig. 1 shows the OM images of the base metal (BM) and FSP samples. Many micron-sized irregular and polygonal particles mainly containing Mn, Si and Fe determined by energy-dispersive spectroscopy were observed in the BM (Fig. 1a). FSP resulted in the significant breakup of the micron-sized particles, and more uniform distribution of particles in the Al matrix (Fig. 1b). Similarly phenomenon was also reported in other Al alloys after FSP [19].

Fig. 2 shows the microstructures of the BM and FSP samples of AA 6082-T4 obtained by EBSD. An incomplete recrystallization structure composed of elongated deformed grains and recrystallized equiaxed grains with sizes below 5 μm were observed in the BM (Fig. 2a). The ultrafine grained (UFG) structure with an average grain size of 0.8 μm was observed in the FSP sample as shown in Fig. 2b. FSP with low rotation rate has been proven to be an effective method of reducing heat input [20,21]. Therefore, the coarsening of recrystallized grains was inhibited during FSP in the present study. The fraction of high angle gain boundaries (HAGBs, misorientation angle > 15°) in the FSP sample was measured to be 90% (Fig. 2d). This fraction is obviously larger than that of the BM, which has a HAGB fraction of about 64% (Fig. 2c).

Fig. 3 shows the TEM images of the BM and FSP samples. The metastable β″ phase, which was characterized by needle-like shape, and low density of dislocations were observed in the BM (Fig. 3a). Many rod-like precipitates (β′ phase) were observed in the FSP sample, and some of them were located at boundaries of UFG.

Heat was generated from the severe friction between the tool and the workpiece during the plastic deformation of FSP. During FSP with high rotation rate, the temperature in the nugget zone can reach as high as 753 K, which was sufficient to dissolve the metastable phase [22]. In the present study, the dissolution of metastable phase was suppressed because of the low heat input. However, the thermo-mechanical coupling effects promoted the transformation of β″ into β′ phase during FSP with 200 rpm.

Fig. 4a shows the engineering stress–strain curves of the BM and FSP samples. Compared with the BM, the FSP sample exhibited slightly decreased yield strength (YS). An analysis of microstructures revealed that two competing effects of FSP on the YS of AA 6082-T4: (i) hardening by grain refinement and more uniform distribution and higher density of micron-sized particles; and (ii) softening by disappearance of metastable β″ phase. The net effect resulted in slight decrease in the YS after FSP.

Compared with the BM, the FSP sample exhibited higher ductility and ultimate strength (UTS). This is mainly attributed to the higher work hardening capability as shown in the true stress–strain curves (Fig. 4b). The equilibrium GBs, low density of dislocations, and high density of particles in the FSP sample led to excellent dislocation

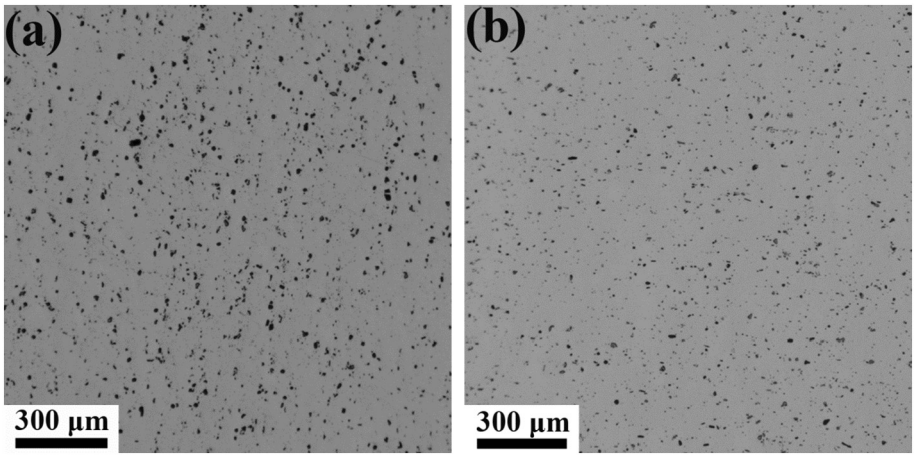

Fig. 1. OM images of (a) BM and (b) the center of FSP sample.

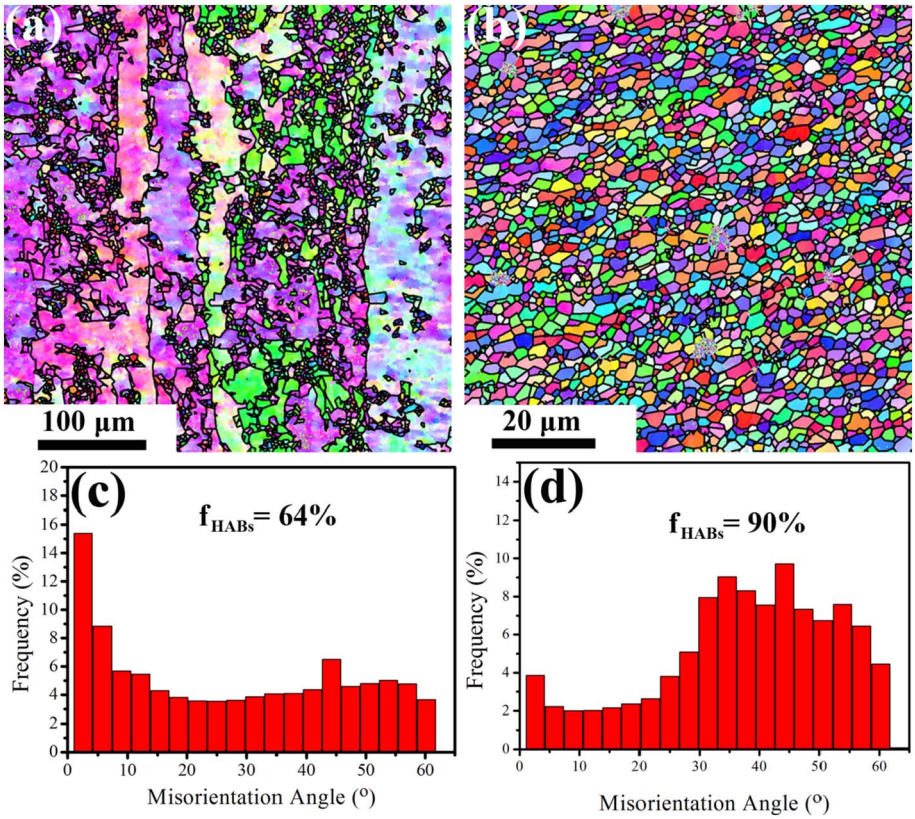

Fig. 2. EBSD maps showing grain structure of (a) BM, (b) the center of FSP sample, and boundary misorientation angle distribution of (c) BM, (d) the center of FSP-200.

accumulation capability during tensile process, thereby achieving improved work hardening capability [23,24].

The fracture surfaces of the BM and FSP samples are shown in Fig. 5. Compared with those of the BM, the fracture surfaces of the FSP sample exhibited finer and more homogenous dimples due to the finer and more homogenous grains of this sample. This structure characteristics of the FSP sample led to that the strain localization could be prevented by redistribution of the stresses during tension, thereby achieving considerable elongation before failure [25].

Fig. 6 shows the strain amplitude dependent damping properties of the BM and FSP samples. The room-temperature damping capacity of the BM and FSP samples was improved with increasing strain amplitude in the general trend. The strain amplitude could be divided into two regions: Region 1 with strain of below 2×10^{-2}, and Region 2 with strain of above 2×10^{-2}.

In Region 1, the damping capacity of the FSP sample was slightly lower than that of the BM. FSP resulted in the annihilation of dislocation lines. So, the FSP sample exhibited a weakened room-temperature damping capacity at low strain amplitude due to less mobile dislocations, according to the Granato–Lücke model [11].

In Region 2, the FSP sample exhibited an optimized room-temperature damping capacity, which is attributed to the following three factors. First, for particle-reinforced AMMCs, it was reported that the density of mobile dislocations near particle-matrix interfaces increased steeply with the increase of strain, and large numbers of mobile dislocations could improve the room-temperature damping capacity [26]. Fig. 7 shows the TEM images of the FSP sample after strain amplitude dependent damping test. High density of dislocations was observed near the particles-Al matrix interfaces (Fig. 7a). Compared with the BM, the FSP sample showed higher density of particles, due to the breakup of the micron-sized particles during FSP. Thus more dislocations were produced in the FSP samples during damping testing at high strain amplitudes, resulting in improved damping capacity.

Second, when the strain amplitude exceeded a certain value, the

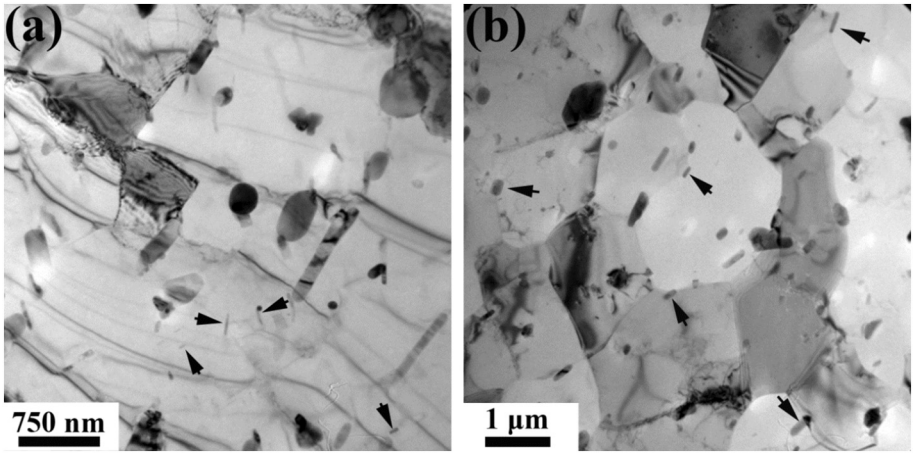

Fig. 3. TEM images of (a) BM and (b) FSP sample. Arrows in (a) denote needle-like precipitates. Arrows in (b) denote precipitates located at GBs.

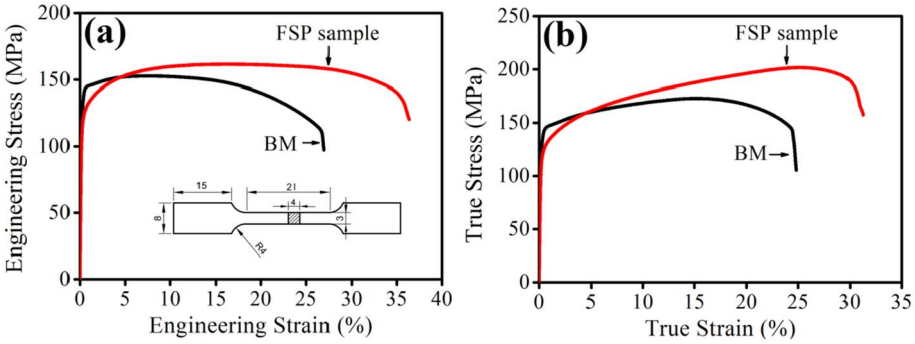

Fig. 4. (a) Engineering and (b) true stress–strain curves of BM and FSP sample. The inset shows the dimension of tensile specimens.

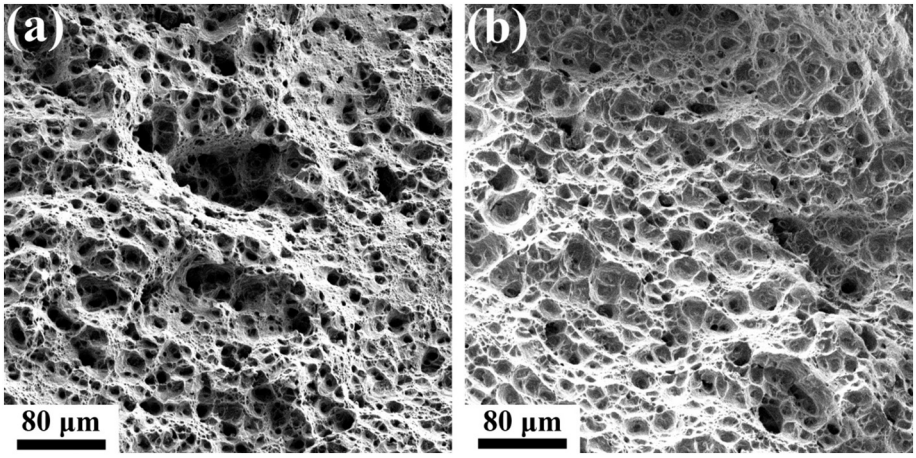

Fig. 5. Fracture surfaces of (a) BM and (b) FSP sample.

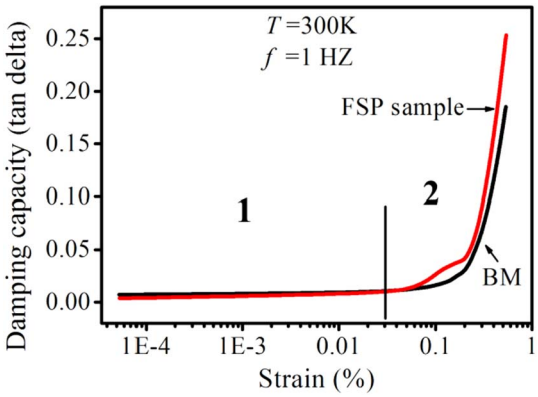

Fig. 6. Strain amplitude dependent damping capacity of BM and FSP sample.

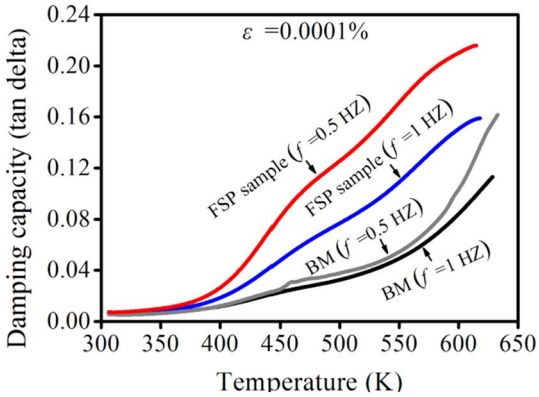

Fig. 8. Temperature dependent damping capacity of BM and FSP sample.

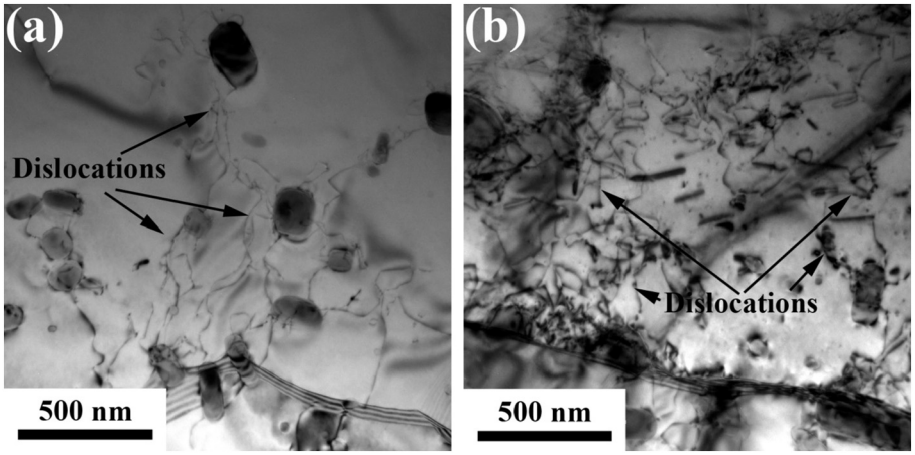

Fig. 7. TEM images of FSP sample after strain amplitude dependent damping test: (a) micron-sized irregular and polygonal particles and (b) pinning of nano-sized precipitates on dislocations.

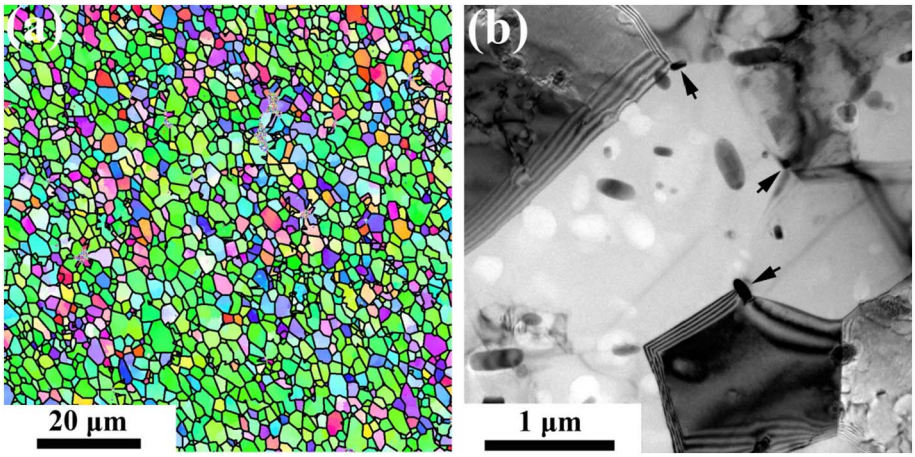

Fig. 9. (a) EBSD map and (b) TEM image of FSP sample after temperature dependent damping test with 1 Hz.

dislocations break away from the weak pinning points, but were still pinned by strong pinning points, such as precipitates [12,13]. As shown in Fig. 7b, the dislocations were pinned by the nano-sized precipitates in the FSP sample after strain amplitude dependent damping test. The coherent β″ phase with more significant pinning role on dislocation than the semi-coherent or incoherent phases [27], was transformed into β′ phase during FSP. Thus, the effect of strong pinning points was weakened in the FSP sample.

Third, high density of GBs was obtained in the FSP sample due to the grain refinement. Similar to the dislocations, GBs as a crystal lattice defect can also contribute to the damping properties. Once the strain amplitude exceeds a critical value, the vibration of GBs occurs, resulting in increased internal friction. Therefore, the FSP sample exhibited excellent room-temperature damping capacity at high strain amplitudes.

Fig. 8 shows the variation of damping capacity with temperature and frequency for the BM and FSP samples. The damping capacity was increased with decreasing frequency. The numbers of mobile dislocations in alloys increased with decreasing frequency at a constant temperature and amplitude, because more pinned dislocations could be activated at the low frequency stress. Therefore, higher damping capacity was obtained during low-frequency vibration [11]. The damping capacity was improved with increasing temperature due to that the viscous flow at GBs would convert mechanical energy into thermal energy as a result of internal friction at GBs [28]. The damping peaks at 460 K were observed in temperature dependent damping curves for the FSP sample. Yang et al. [29] and Cai et al. [30] associated the damping peak at about 450 K with the GB relaxation in Al. Thus, GB sliding was the main damping mechanism of the FSP sample after 460 K in this study.

Compared with the BM, the FSP sample showed much higher high-temperature damping capability. The microstructure of the FSP sample was characterized by equiaxed UFG structure, random grain misorientation distribution, predominant high angle GBs, and low density of dislocations (Figs. 2b, d and 3b). This special microstructure always contributes to excellent GB sliding capacity and superplasticity in high temperature [14–18].

Fig. 9 shows the microstructure of the FSP sample after temperature dependent damping test. The structure with equiaxed grains was retained in the FSP sample after test, and the average grain size of this sample was about 1.6 μm (Fig. 9a), which was slightly higher than that of the FSP sample before damping test (Fig. 2b). Fig. 9b shows the some precipitates were located at GBs. These precipitates can effectively inhibit the growth of fine grains at high temperature and improve the GB sliding capacity of Al alloys [31]. Thus, the high-temperature damping capacity of AA 6082-T4 was improved by FSP with low rotation rate.

4. Conclusions

In this study, the damping capacity of AA 6082-T4 at both room temperature and high-temperature were simultaneously improved by FSP with 200 rpm. This was attributed to the special microstructure characterized by equiaxed UFG structure, low density of dislocations, uniform distribution of micron-sized particles, high density of nano-sized precipitates located at GBs, and low amount of solute atoms in solid solution. Furthermore, the ductility and UTS of AA 6082-T4 alloy were also improved by FSP, due to the higher work hardening capability and more homogenous microstructures in the FSP sample. This work provides an effective strategy to improve the damping capacity of commercial Al alloys without sacrificing their mechanical properties.

Acknowledgements

This work was funded by the National Natural Science Foundation of China (No. 51601045), Guangxi Natural Science Foundation (No. 2015GXNSFBA139238), and the Guangxi ‘Bagui’ Teams for Innovation and Research.

References

[1] D.Q. Wan, Near spherical α-Mg dendrite morphology and high damping of low-temperature casting Mg–1wt.%Ca alloy, Mater. Charact. 62 (2011) 8–11.
[2] Y.J. Zhang, N.H. Ma, H.W. Wang, X.F. Li, Study on damping behavior of A356 alloy after grain refinement, Mater. Des. 29 (2008) 706–708.
[3] J. Liu, P. Yao, N.Q. Zhao, C.S. Shi, H.J. Li, X. Li, D.S. Xi, S. Yang, Effect of minor Sc and Zr on recrystallization behavior and mechanical properties of novel Al–Zn–Mg–Cu alloys, J. Alloys Compd. 657 (2016) 717–725.
[4] M.C. Gui, D.B. Wang, J.J. Wu, G.J. Yuan, C.G. Li, Deformation and damping behaviors of foamed Al–Si–SiC_p composite, Mater. Sci. Eng. A 286 (2000) 282–288.
[5] S. Madeira, G. Miranda, V.H. Carneiro, D. Soares, F.S. Silva, O. Carvalho, The effect of SiC_p size on high temperature damping capacity and dynamic Young's modulus of hot-pressed AlSi–SiC_p MMCs, Mater. Des. 93 (2016) 409–417.
[6] N. Srikanth, H.K.F. Calvin, M. Gupta, Effect of length scale of alumina particles of different sizes on the damping characteristics of an Al–Mg alloy, Mater. Sci. Eng. A 423 (2006) 189–191.
[7] Y.J. Zhang, N.H. Ma, H.W. Wang, Effect of Ti and Mg on the damping behavior of in situ aluminum composites, Mater. Lett. 61 (2007) 3273–3275.
[8] D.R. Ni, J.J. Wang, Z.Y. Ma, Shape memory effect, thermal expansion and damping property of friction stir processed $NiTi_p$/Al composite, J. Mater. Sci. Technol. 32 (2016) 162–166.
[9] B.H. Luo, Z.H. Bai, Y.Q. Xie, The effects of trace Sc and Zr on microstructure and internal friction of Zn–Al eutectoid alloy, Mater. Sci. Eng. A 370 (2004) 172–176.
[10] Z.H. Ma, F.S. Han, J.N. Wei, J.C. Gao, Effects of macroscopic defects on the damping behavior of aluminum and Zn–27 Pct Al alloy, Metall. Mater. Trans. A 32 (2000) 2001–2657.
[11] J.F. Wang, R.P. Lu, W.W. Wei, X.F. Huang, F.S. Pan, Effect of long period stacking ordered (LPSO) structure on the damping capacities of Mg–Cu–Mn–Zn–Y alloys, J. Alloys Compd. 537 (2012) 1–5.
[12] X.S. Hu, K. Wu, M.Y. Zheng, Effect of heat treatment on the stability of damping capacity in hypoeutectic Mg–Si alloy, Scr. Mater. 54 (2006) 1639–1643.
[13] Z.Y. Zhang, X.Q. Zeng, W.J. Ding, The influence of heat treatment on damping response of AZ91D magnesium alloy, Mater. Sci. Eng. A 392 (2005) 150–155.

[14] F.C. Liu, Z.Y. Ma, F.C. Zhang, High strain rate superplasticity in a micro-grained Al–Mg–Sc alloy with predominant high angle grain boundaries, J. Mater. Sci. Technol. 28 (2012) 1025–1030.
[15] F.C. Liu, Z.Y. Ma, L.Q. Chen, Low-temperature superplasticity of Al–Mg–Sc alloy produced by friction stir processing, Scr. Mater. 60 (2009) 968–971.
[16] I. Charit, R.S. Mishra, Low temperature superplasticity in a friction-stir-processed ultrafine grained Al–Zn–Mg–Sc alloy, Acta Mater. 53 (2005) 4211–4223.
[17] Z.Y. Ma, F.C. Liu, R.S. Mishra, Superplastic deformation mechanism of an ultrafine-grained aluminum alloy produced by friction stir processing, Acta Mater. 58 (2010) 4693–4704.
[18] Z.Y. Ma, S.R. Sharma, R.S. Mishra, Effect of multiple-pass friction stir processing on microstructure and tensile properties of a cast aluminum–silicon alloy, Scr. Mater. 54 (2006) 1623–1626.
[19] Z.Y. Ma, Friction stir processing technology: a review, Metall. Mater. Trans. A 39 (2008) 642–658.
[20] C.Y. Liu, B. Qu, P. Xue, Z.Y. Ma, K. Luo, M.Z. Ma, R.P. Liu, Fabrication of large-bulk ultrafine grained 6061 aluminum alloy by rolling and low-heat-input friction stir welding, J. Mater. Sci. Technol. (2017), http://dx.doi.org/10.1016/j.jmst.2017.02.008 (in press).
[21] P. Xue, B.L. Xiao, Q. Zhang, Z.Y. Ma, Achieving friction stir welded pure copper joints with nearly equal strength to the parent metal via additional rapid cooling, Scr. Mater. 64 (2011) 1051–1054.
[22] R.S. Mishra, Z.Y. Ma, Friction stir welding and processing, Mater. Sci. Eng. R 50 (2005) 1–78.
[23] Y.T. Zhu, X.Z. Liao, Nanostructured metals: retaining ductility, Nat. Mater. 3 (2004) 351–352.
[24] Y.H. Zhao, X.Z. Liao, S. Cheng, E. Ma, Y.T. Zhu, Simultaneously increasing the ductility and strength of nanostructured alloys, Adv. Mater. 18 (2006) 2280–2283.
[25] D. Yadav, R. Bauri, Effect of friction stir processing on microstructure and mechanical properties of aluminium, Mater. Sci. Eng. A 539 (2012) 85–92.
[26] H. Sekine, R. Chen, A combined microstructure strengthening analysis of SiCp/Al metal matrix composites, Composites 26 (1995) 183–188.
[27] C.D. Lee, Damping properties on age hardening of Al–7Si–0.3Mg alloy during T6 treatment, Mater. Sci. Eng. A 394 (2005) 112–116.
[28] H. Watanabe, T. Mukai, M. Sugioka, K. Ishikawa, Elastic and damping properties from room temperature to 673 K in an AZ31 magnesium alloy, Scr. Mater. 51 (2004) 291–295.
[29] Z.Q. Yang, J. Chen, L.L. He, H.T. Cong, H.Q. Ye, Microstructure and grain boundary relaxation in ultrafine-grained Al/Al oxide composites, Acta Mater. 57 (2009) 3633–3644.
[30] B. Cai, Q.P. Kong, P. Cui, H.T. Cong, X.K. Sun, Internal friction of nanocrystalline aluminum prepared by plasma evaporation and compaction, Scr. Mater. 44 (2001) 1043–1048.
[31] F.C. Liu, Z.Y. Ma, Achieving exceptionally high superplasticity at high strain rates in a micrograined Al–Mg–Sc alloy produced by friction stir processing, Scr. Mater. 59 (2008) 882–885.